AFRL-AFOSR-VA-TR-2020-0191

PECASE: Parity-Time Symmetric Nanophotonic Materials and Metamaterials

Jennifer Dionne
LELAND STANFORD JUNIOR UNIVERSITY

08/31/2020
Final Report

DISTRIBUTION A: Distribution approved for public release.

Air Force Research Laboratory
AF Office Of Scientific Research (AFOSR)/ RTB1
Arlington, Virginia 22203
Air Force Materiel Command

REPORT DOCUMENTATION PAGE

Form Approved
OMB No. 0704-0188

1. REPORT DATE *(DD-MM-YYYY)*
09-10-2020

2. REPORT TYPE
Final Performance

3. DATES COVERED *(From - To)*
31 Oct 2014 to 30 Oct 2019

4. TITLE AND SUBTITLE
PECASE: Parity-Time Symmetric Nanophotonic Materials and Metamaterials

5a. CONTRACT NUMBER

5b. GRANT NUMBER
FA9550-15-1-0006

5c. PROGRAM ELEMENT NUMBER
61102F

6. AUTHOR(S)
Jennifer Dionne

5d. PROJECT NUMBER

5e. TASK NUMBER

5f. WORK UNIT NUMBER

7. PERFORMING ORGANIZATION NAME(S) AND ADDRESS(ES)
LELAND STANFORD JUNIOR UNIVERSITY
450 SERRA MALL
STANFORD, CA 94305-2004 US

8. PERFORMING ORGANIZATION REPORT NUMBER

9. SPONSORING/MONITORING AGENCY NAME(S) AND ADDRESS(ES)
AF Office of Scientific Research
875 N. Randolph St. Room 3112
Arlington, VA 22203

10. SPONSOR/MONITOR'S ACRONYM(S)
AFRL/AFOSR RTB1

11. SPONSOR/MONITOR'S REPORT NUMBER(S)
AFRL-AFOSR-VA-TR-2020-0191

12. DISTRIBUTION/AVAILABILITY STATEMENT
A DISTRIBUTION UNLIMITED: PB Public Release

13. SUPPLEMENTARY NOTES

14. ABSTRACT
The aim of the program was to develop a new class of nanoscale optical components and devices capable of lossless, asymmetric, nonlinear, and non-reciprocal light propagation across wavelength and sub-wavelength scales. Key Accomplishments from 2014 to 2019 included: (1) Design of nanoscale optical diodes; (2) Design of nanoscale optical isolators; (3) The first high-quality factor phase gradient metasurfaces; (4) Design of PT-symmetric plasmonic apertures for polarization rotation; (5) Design of broadband non-Hermitian metamaterials; and (6) Enantioselective optical trapping. In the final year of the grant, key accomplishments include:
1. Design and fabrication of the first high-quality (high-Q) factor phase gradient metasurfaces. These metasurfaces have Q-factors in the thousands, and enable arbitrary optical transfer functions like beam-steering, beam-splitting, and lensing. They lay the foundation for efficienct nonlinear and electro-optic modulation of metasurfaces.
2. Design of power-limiting lenses based on high-Q metasurfaces. We designed high-Q lenses, and use the intrinsic nonlinearity of Si to modulate the focal intensity and focal length. These lenses operate in the near-infrared, and several high-Q resonances can be embedded in the structure for multiplexed operation.
3. A new method for self-isolated lasing, based on high-Q chiral metasurfaces. We designed a sub-micron-thick lasing cavity that is inherently protected from reflections. This device utilizes spin-selective selection rules in Raman lasers with a circularly-polarized pump. A signal with an arbitrary polarization state transmits with amplification in one direction, but its reflection is suppressed by approximately an order of magnitude in the metasurface cavity, resulting in isolation.

15. SUBJECT TERMS
light-matter interactions, nanophotonics, metamaterials, parity-time-symmetric materials, subwavelength, optical devices

Standard Form 298 (Rev. 8/98)
Prescribed by ANSI Std. Z39.18

16. SECURITY CLASSIFICATION OF:			17. LIMITATION OF ABSTRACT	18. NUMBER OF PAGES	19a. NAME OF RESPONSIBLE PERSON POMRENKE, GERNOT
a. REPORT	b. ABSTRACT	c. THIS PAGE			
Unclassified	Unclassified	Unclassified	UU		19b. TELEPHONE NUMBER *(Include area code)* 703-696-8426

Standard Form 298 (Rev. 8/98)
Prescribed by ANSI Std. Z39.18

DISTRIBUTION A: Distribution approved for public release.

PECASE – Title: Parity-time Symmetric Nanophotonic Materials and Metamaterials
J. Dionne, Stanford University
Final Report, Start Date: 10/31/2014, End Date: 10/30/2019
FA9550-15-1-0006

Executive Summary: The aim of the program was to develop a new class of nanoscale optical components and devices capable of lossless, asymmetric, nonlinear, and non-reciprocal light propagation across wavelength and sub-wavelength scales. Key Accomplishments from 2014 to 2019 included: (1) Design of nanoscale optical diodes; (2) Design of nanoscale optical isolators; (3) The first high-quality factor phase gradient metasurfaces; (4) Design of PT-symmetric plasmonic apertures for polarization rotation; (5)
Design of broadband non-Hermitian metamaterials; and (5) Enantioselective optical trapping.
In the final year of the grant, key accomplishments include:

1. Design and fabrication of the first high-quality ("high-Q") factor phase gradient metasurfaces. These metasurfaces have Q-factors in the thousands, and enable arbitrary optical transfer functions like beam-steering, beam-splitting, and lensing. They lay the foundation for efficienct nonlinear and electro-optic modulation of metasurfaces.
2. Design of power-limiting lenses based on high-Q metasurfaces. We designed high-Q lenses, and use the intrinsic nonlinearity of Si to modulate the focal intensity and focal length. These lenses operate in the near-infrared, and several high-Q resonances can be embedded in the structure for multiplexed operation.
3. A new method for self-isolated lasing, based on high-Q chiral metasurfaces. We designed a sub-micron-thick lasing cavity that is inherently protected from reflections. This device utilizes spin-selective selection rules in Raman lasers with a circularly-polarized pump. A signal with an arbitrary polarization state transmits with amplification in one direction, but its reflection is suppressed by approximately an order of magnitude in the metasurface cavity, resulting in isolation.

Funded Students and Postdoctoral Fellows for 2018-2019:
Dr. David Barton, Materials Science (defended Ph.D., Spring 2020); now postdoctoral fellow at Harvard in Capasso/Loncar Labs
Dr. Mark Lawrence, postdoctoral fellow; now faculty in Electrical Engineering at Washington University in St. Louis
Jefferson Dixon, Graduate student, Mechanical Engineering, Stanford University
Elissa Klopfer, Graduate student, Materials Science, Stanford University
Sahil Dagli, Graduate student, Materials Science, Stanford University

Previously-funded Students and Postdoctoral Fellows:
Dr. Yang Zhao, now faculty at UIUC
Dr. Brian Baum, now at Intel
Dr. Hadiseh Alaeian, Electrical Engineering (defended Ph.D., Fall 2015); now faculty at Purdue
Dr. Tarun Narayan, Materials Science (defended Ph.D. Fall 2016; awarded best PhD dissertation); now fellow at Cyclotron Road

Goal: Develop a new class of nanoscale optical components and devices capable of lossless, asymmetric, nonlinear, and non-reciprocal light propagation across wavelength and sub-wavelength scales

Results from final funded year, 2018-2019

Achieving resonant and unidirectional light propagation is essential for integrated photonic communication and computation platforms. To observe asymmetric and nonreciprocal transport, time reversal symmetry must be broken. Unfortunately, mechanisms which violate time reversal symmetry, such as magneto-optic effects, are generally very weak, leading to bulky optical isolators. Our project aimed to develop nanoscale devices capable of asymmetric and non-reciprocal optical transport. In our final year of the grant, key accomplishments include:

1. **Design and fabrication of the first high-quality ("high-Q") factor phase gradient metasurfaces.** These metasurfaces have Q-factors in the thousands, and enable arbitrary optical transfer functions like beam-steering, beam-splitting, and lensing. They lay the foundation for efficienct nonlinear and electro-optic modulation of metasurfaces.
2. **Design of power-limiting lenses based on high-Q metasurfaces**. We designed high-Q lenses, and use the intrinsic nonlinearity of Si to modulate the focal intensity and focal length. These lenses operate in the near-infrared, and several high-Q resonances can be embedded in the structure for multiplexed operation.
3. **A new method for self-isolated lasing, based on high-Q chiral metasurfaces.** We designed a sub-micron-thick lasing cavity that is inherently protected from reflections. This device utilizes spin-selective selection rules in Raman lasers with a circularly-polarized pump. A signal with an arbitrary polarization state transmits with amplification in one direction, but its reflection is suppressed by approximately an order of magnitude in the metasurface cavity, resulting in isolation.

Results from 2018-2019

1. High-Q Phase Gradient Metasurfaces

Metasurfaces enable nearly arbitrary transformations to incoming and outgoing light based on spatially arrayed subwavelength dielectric or plasmonic nanoantennas. However, weak light-matter interactions limit the ability to access nonlinear, nonreciprocal, and reconfigurable devices, significantly limiting their potential applicability. High quality factor (high-Q) structures, such as photonic crystals and on-chip ring resonators, enhance light-matter interaction by dramatically increasing photon lifetimes and reducing the tuning bandwidth needed for reconfigurability. Previously demonstrated metasurfaces have intrinsically low quality factors (~10), as they rely on standard lower order Mie modes that quickly scatter light into the radiation continuum. We have combined the power of high-Q optical cavities and phase gradient metasurfaces, experimentally demonstrating the first high-Q phase gradient metasurfaces. The generality of our design and results enable a plethora of novel tunable, reconfigurable, and nonlinear flat optical devices, including light detection and ranging (for example LIDAR), light fidelity (LiFi), and quantum and non-reciprocal optical communication.

To design the broadband phase gradient response, we choose 600 nm tall silicon nanobars spaced by 707 nm as our metasurface element. This acts as a Huygens metasurface, allowing for full wavefront (i.e. 2π) phase control, while maintaining high transmittance. For our beamsteering designs, we specifically use

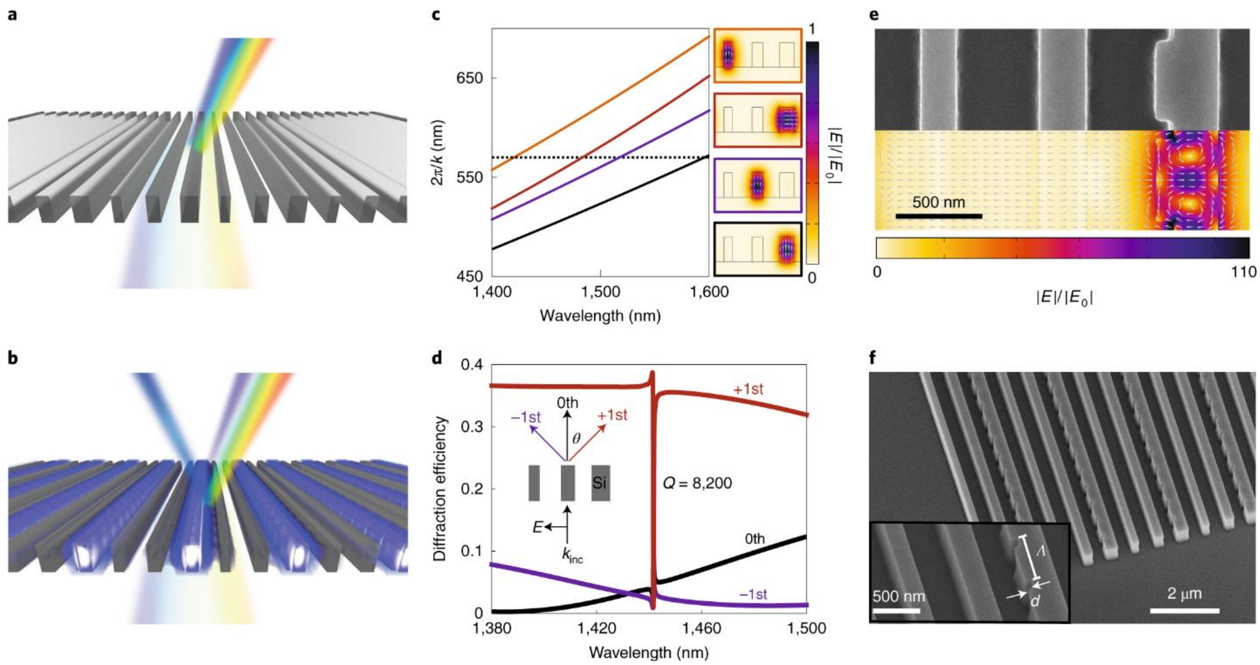

Fig. 1: Conceptual and numerical design of high-Q phase gradient metasurfaces. ***a***, *Schematic illustrating broadband beam steering with a Mie resonant phase gradient metasurface.* ***b***, *Schematic illustrating strong light localization and modified diffraction after perturbation of phase gradient metasurface shown in* ***a***. ***c***, *Waveguide dispersion for phase gradient metasurface shown in a. Left: guided-mode wavelength ($2\pi/k$) plotted against free-space wavelength (λ), with dashed line denoting $2\pi/k = 570$ nm. Right: electric field distributions, colour coded to match dispersion plot. Arrows represent electric field polarization. $|E|/|E_0|$ denotes the amplitude of the electric E field normalized by the incident field amplitude.* ***d***, *Simulated diffraction spectra for periodically perturbed phase gradient metasurface. Inset: schematic showing illumination and diffraction configuration, colour coded to match spectra. e, Top: SEM image of metasurface fabricated with nominal dimensions matching those in d. Bottom: simulated electric near-field distribution at the GMR centre wavelength corresponding to that in d. Arrows represent electric field polarization. f, Angled SEM images, with enlargement in inset, of fabricated phase gradient metasurfaces demonstrating uniform patterning and minimal sidewall tapering. Perturbation period (Λ) and depth (d) are labelled.*

nanobars with heights of 600 nm, spacing of 707 nm, and a 3-bar supercell with widths 190, 260, and 350 nm. To generate a high quality factor response, we include subtle perturbation into individual nanoantennas to generate high-Q dipole resonances. To this end, we note that each nanoantenna maintains a degree of translational symmetry (Fig. 1a), and therefore each element can also act as a waveguide. Fig. 1c, shows the calculated waveguide dispersion for the first four modes within the metasurface. These modes possess larger momentum than free-space radiation and therefore fully bound to their respective nanoantennas. This momentum mismatch can be bridged by introducing a series of periodic notches with period Λ along the entire bar. Then, light will leak back out to free space appearing as a guided-mode resonance (GMR) in the diffraction spectra when Λ equals the guided-mode wavelength. A numerical example of such a resonance, for 100-nm-deep, 100-nm-long notches placed within the largest bar every 570 nm, is given in Fig. 1d. Efficient beam steering to the $+1^{st}$ order occurs across most of the plotted spectral range, while a GMR close to $\lambda = 1{,}440$ nm creates a narrow reflective band with a Q-factor of ~8,200. Crucially, our silicon nanobars here maintain a dipole radiation pattern in the plane of diffraction, giving the ability to shape wavefronts.

We fabricated the designed structures in a Silicon on Sapphire platform. Care must be taken in the fabrication to generate structures that are as uniform as possible, both along the bar direction and phase gradient direction. If the perturbations are not identical within a bar, the deviations from the design act as radiative scattering centers, decreasing both the contrast and the quality factor. Additionally, each bar with perturbations need to be as similar as possible to each other, such that the resonance wavelength of each bar (and scattered phase) is as identical as possible. We fabricate devices with areal dimensions 300 micron x 300 micron for ease of characterization, which means that ~140 resonators must have their resonant frequencies and quality factors match to observe anything in the far field. A representative scanning electron microscope (SEM) image of one such sample is shown in Fig. 1f, annotated with the two parameters that we varied experimentally—notch depth d and period Λ.

We characterize these devices by illuminating them at normal incidence through the substrate with a collimated white-light laser and measuring transmission with an imaging spectrometer. The Fourier plane spectral map of a metasurface with Λ = 570 nm and d = 100 nm shows strong preferential scattering into the +1st diffraction, verifying the linear phase gradient design (Fig. 2a). A narrow dip in the +1st diffraction near 1,440 nm reveals the presence of a GMR. Our scheme does not rely on large areas and

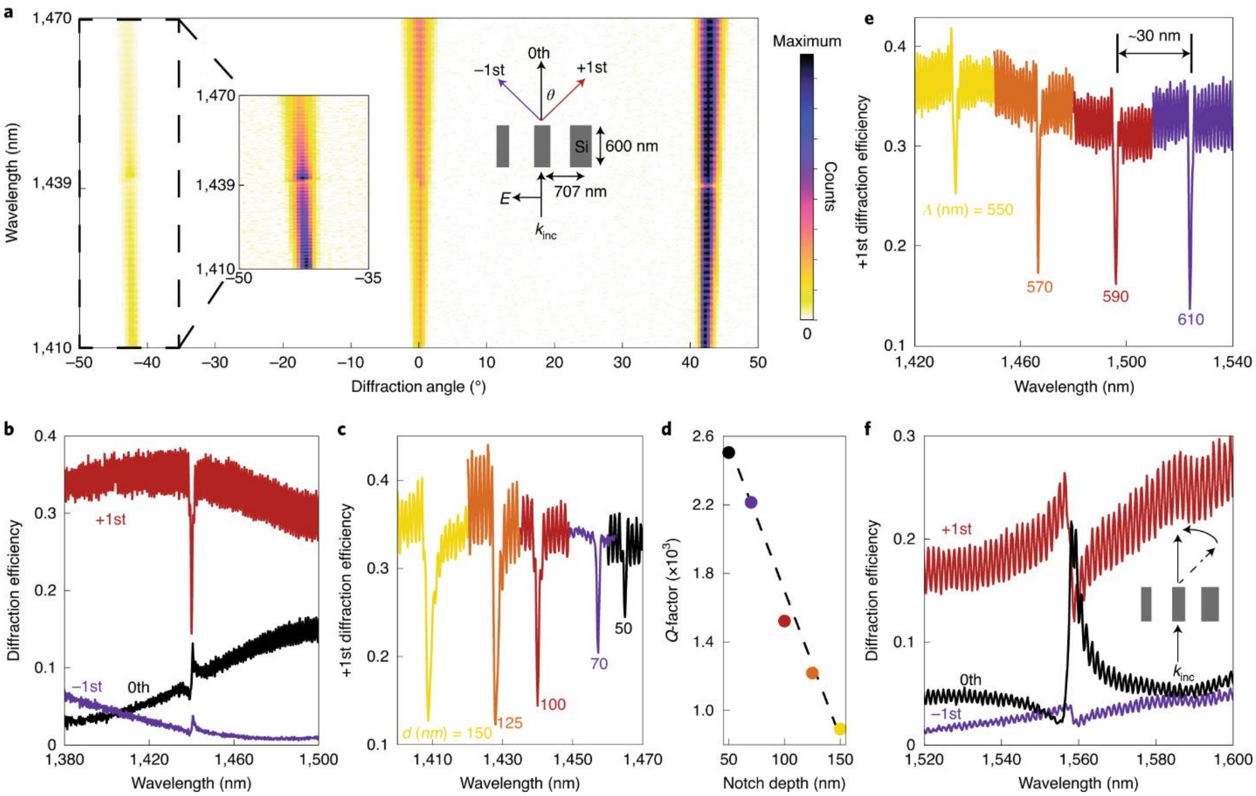

Fig. 2: Experimental demonstration of high-Q phase gradient metasurface beam steering. ***a****, Fourier plane spectral image of beam-steering phase gradient metasurface, with Λ = 570 nm and d = 100 nm. Left inset: self-normalized -1*st *diffraction order. Right inset: schematic showing illumination and diffraction configuration.* ***b****, Diffraction spectra for sample used in* ***a. c****, +1st diffraction spectra for metasurfaces, with perturbation depth d decreasing from 150 to 50 nm.* ***d****, Extracted quality factors from* ***c****, colour coded to match spectra. The dashed line was drawn as a visual guide.* ***e****, +1st diffraction spectra for metasurfaces with d = 70 nm and varying perturbation period Λ, spanning 550–610 nm in 20-nm increments. The purple curve in* ***c*** *and orange curve in* ***e*** *are from structures of nominally identical dimensions but were patterned on different samples.* ***f****, Lower-frequency GMR measured in metasurface, with Λ = 570 nm and d = 100 nm and measurements performed as in* ***b****.*

have fabricated metasurfaces of only 7 μm in the phase gradient direction (corresponding to a total of ten metasurface elements) without influencing the high-Q resonant feature.

To better quantify the response of our metasurfaces, we also recorded the real-space spectral image of each diffraction order independently. Using this approach, Fig. 2b shows the normalized spectra from the sample used in Fig. 2a. Apart from the constant oscillations arising from Fabry–Perot resonance in the substrate, we find excellent agreement between Fig. 2b and the numerical data presented in Fig. 1d. A quality factor of 1,500 has been extracted for this mode. In Fig. 2c we fix $\Lambda = 570$ nm and plot relevant portions of the +1st diffraction spectra with the notch depth d swept from 150 nm (yellow curve) to 50 nm (black curve). As d drops to 50 nm we observe a red shift of approximately 60 nm as the GMR approaches the band crossing point of an ideal, or unnotched, waveguide (∼1,500 nm) (Fig. 1c). More importantly, Q is seen to increase from 900 to 2,500. Aside from line width, we also investigated the ability to systematically tune the spectral position of the GMR. Fixing d = 70 nm, Fig. 2e displays the relevant portions of the +1st order diffraction efficiency for $\Lambda = 550$ nm (yellow curve) to 610 nm (purple curve), in 20-nm increments. The resonant centre wavelength by approximately 30 nm for every 20-nm increase in period without substantially impacting the background phase gradient profile. Since the perturbations are inserted into the largest bar, a second GMR exists at a longer wavelength, corresponding to free-space coupling into a vertically polarized waveguide mode (see the black dispersion curve in Fig. 1c). Figure 2f displays the diffraction spectra of a metasurface near $\lambda = 1{,}560$ nm. The different phase relationship between the broad background and localized mode produces a more asymmetric Fano line shape in the +1st diffraction order; the narrowband response is dominated by direct transmission while off-resonance the structure steers light to ∼45°.

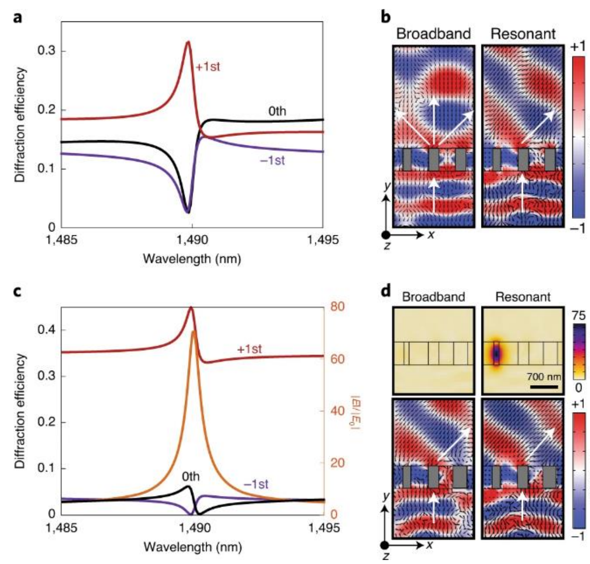

__Fig. 3: Narrowband and slow-light beam steering. a__, Simulated diffraction spectra of narrowband beam-steering metasurface with asymmetric perturbations placed in the thinnest bar. Curve colours are chosen to match the schematic in the inset of Fig. 1d. __b__, Magnetic field maps corresponding to __a__, at λ = 1,495 nm (broadband) and λ = 1,489.9 nm (resonant). __c__, Simulated diffraction spectra of slow-light beam-steering metasurface, with identical geometry as in __a__ for the thinnest bar but different neighbouring bar widths. The orange curve represents peak electric field amplitude (right y axis), while remaining curves represent diffraction orders with colours chosen to match the schematic in the inset of Fig. 1d. __d__, Electric field amplitude (top) and magnetic field (bottom) maps corresponding to __c__, at λ = 1,495 nm (broadband) and λ = 1,490 nm (resonant). Shorter arrows overlaid with magnetic fields display the local Poynting vector, while longer arrows highlight the dominant diffraction orders.

We have explored additional opportunities enabled by this design principle. First, we show how relative weights associated with the available diffraction orders can be independently tailored both on and off resonance. Figure 2f shows that high-Q scattering into the directly transmitted beam can be increased while the first diffracted order is suppressed. In Fig. 2a–e, the GMR is approximately an in-plane electric dipole. In contrast, the response shown in Fig. 2f is associated with a vertically polarized electric dipole. Vertical and horizontal dipoles couples differently to both the incident wave and notch symmetry, giving a new degree of freedom in diffraction. While the radiation pattern of a GMR depends predominantly on the notch dimensions, the overall metasurface scattering is decided by the interplay between the GMR and the background phase profile. We use this to numerically demonstrate two additional spectral transfer functions of the three-bar design: narrowband beam steering and slow-light beam steering. To achieve these functions, we switch to a vertically polarized electric dipole GMR. We also decrease the width of the notched bar to 210 nm, thereby changing the background Mie scattered phase associated with the narrow resonance and adjusting its line shape. A key property of a vertical electric dipole is that it radiates symmetrically about the vertical axis, meaning that such a mode cannot be excited by a plane wave travelling in the vertical direction unless the metasurface breaks that inversion symmetry. The phase of light emitted to the left and right can be controlled by tuning the relative depth of notches placed on the left and right sides of the bar. This allows interference between the resonant scattering and background diffraction to be engineered separately for different diffracted directions. In contrast, the in-plane mode exhibits very different behaviour with the angular intensity of emission depending on notch symmetry.

Taking advantage of these insights, we placed periodic notches of period 635 nm into both sides of the 210-nm-wide bar. The notches were 36-nm deep, 150-nm long on the left (negative x direction) and 44-nm deep, 150-nm long on the right (positive x direction). We find that placing this structure between bars of width 275 and 280 nm produces sharp dips in both −1st and 0th diffraction orders (Fig. 3a, purple and black curves) but a narrow peak in the +1st diffraction order (Fig. 3a, red curve). As confirmed by the magnetic field profiles and overlaid Poynting vectors (Fig. 3b), this combination results in the metasurface exhibiting balanced diffraction off-resonance but steers the incident wave to ∼45° close to the GMR ($\lambda = 1{,}489.9$ nm). In Fig. 3c, we take the structure from Fig. 3a and replace the 275-nm-wide bar with a 370-nm-wide bar. Here, spectral variation in the diffraction around the GMR is almost entirely removed while maintaining the strong spectrally narrow field enhancement associated with high-Q resonance. Similarly, the magnetic field profiles show very little change in the beam-steering response with wavelength, while maps of electric field amplitude reveal a dramatic enhancement (exceeding 75×) within the perturbed bar on-resonance (Fig. 3d). Accordingly, with our high-Q metasurface approach, the optical transfer function, near-field intensity, and resonant line shape can all be rationally designed.

While nanoantennas represent an exciting development for optical science, researchers typically face a trade-off between antenna size in relation to wavelength and resonant lifetime. In shaping diffraction using high-Q nanoantennas of subwavelength cross-section in the diffraction plane, we provide experimental evidence to suggest that this trade-off may not, in fact, be fundamental. **Our results point to the possibility that highly resonant and highly compact features, once in the purview only of on-chip photonics, can be rationally designed to coincide with an arbitrarily chosen electromagnetic wavefront.** This design methodology can be extended to more complicated phase transformations such lenses and holograms, as described below. Much higher Q-factors (10^4–10^5) should be achievable with refined fabrication processes and improved imperfection-tolerant designs. **By enabling resonant near-field intensity and line shape to be engineered in conjunction with arbitrary wavefront transformations, we envision an impact by high-Q phase gradient metasurfaces on any AFOSR-relevant challenge requiring efficient diffractive optical switching or tuning and low nonlinear thresholds; specific applications include light detection and ranging (for example LIDAR), light fidelity (LiFi), and quantum and non-reciprocal optical communication.**

2. Dynamic focusing via an ultrathin Kerr-nonlinear high-Q metalens

Metasurface lenses (hereafter, ‘metalenses’) are emerging as key components for next-generation miniaturized and lightweight imaging, sensing, and computation systems. They promise applications including compact, high grade imaging for cameras and displays, on chip biomedical diagnostics, and next generation augmented and virtual reality (AR/VR) devices. Still, to date, most metalens designs are static, with their function being fixed once fabricated. Many current modulation schemes rely on altering the complex refractive index (n) of a device. However since the index change is proportional to the strength of the local electromagnetic field, metasurface modulation depths are generally small, owing to the low quality factor of the constituent nanoantennas. To amplify modulation depths while maintaining a small device footprint, it is crucial to amplify refractive index changes though increased metasurface quality factors.

This year, we designed submicron-thick, ultrahigh quality factor (high-Q) metalenses that enable dynamic modulation of focal length and intensity. These metalenses leverage highly-enhanced electromagnetic fields to increase the modulation depth with even weak Δn effects, without increasing the system footprint. Our design is based on patterned silicon (Si), that achieve a high-Q response based on guided mode resonances (GMR). **We show that this design easily enables Qs in the thousands, and near-field intensity enhancements exceeding 10,000. Utilizing the nonlinear Kerr effect, we theoretically demonstrate modulation of both the focal intensity and focal length with varying incident intensity.**

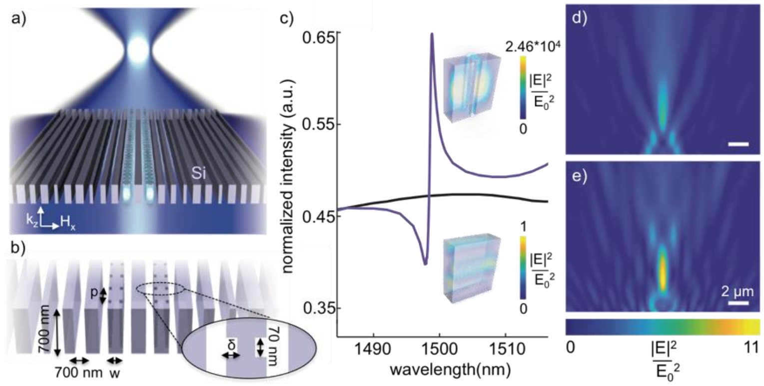

Figure 4: *High-Q metalens geometry and spectral characteristics. a) Schematic of the high-Q lens, illustrating the local field enhancements that arise in the notched bars (here positioned on each side of the lens midpoint), b) geometry of a subset of the high-Q structure, where p=600 nm, δ=50 nm, and w varies for each bar according to Figure S1b, c) spectra of the unnotched (black curve) and notched (purple curve) lenses calculated for the xy plane at the focal spot, 4 μm from the metasurface. The insets show near-field calculations of the w=219 nm nanobars for the notched and unnotched lenses, d) $|E(r)|^2$ field plot for the unnotched lens excited at λ=1499.4 nm and normalized to the mean of the input gaussian field, e) $|E(r)|^2$ field plot for the notched, high-Q lens excited at λ=1499.4 nm and normalized to the mean of the input gaussian field.*

Our cylindrical metalens obeys a hyperboloidal phase profile constructed by 25 discrete Si nanobars. To integrate a high-Q resonance into the diffractive metalens, we introduce subtle periodic perturbations along the length of one pair of nanobars, as illustrated in Figure 4a and b. The nanobars support wave-guided modes; from the perspective of the external plane wave, the continuous waveguide represents a resonator with infinite Q. The inclusion of periodic notches to a nanobar, with the notch period associated with the guided mode wavevector, enables momentum matching and coupling between the guided modes and the external field, and the excitation of the GMR. This GMR supports measurable resonances in the far field. Importantly, excitation of GMRs only occurs for a small range of wavelengths, giving rise to strongly resonant fields and hence a high-Q. For our high-Q metalens design, we include periodic notches in the set of bars adjacent to the lens center.

For an incident intensity of 0.1 mW/μm^2, the spectral response of the notched and un-notched metalenses is shown in Figure 4c. As seen, a high-Q resonance appears for the notched metasurface at a wavelength of λ=1499.4 nm, associated with a Q factor of 3600. Near fields of the nanobars, shown in the insets of Figure 1c, show a maximum enhancement of the notched bar near field intensity of $2.46*10^4$ compared to the unnotched bars. Figure 1d and e confirm the focusing abilities of the low-Q and high-Q metalenses for an incident wavelength 1499.4 nm. Thus, our metasurface design simultaneously achieves strong focusing behavior as well as quality factors two order of magnitude larger than those achieved by other diffractive metasurfaces; to our knowledge, this is the first high-Q metalens design.

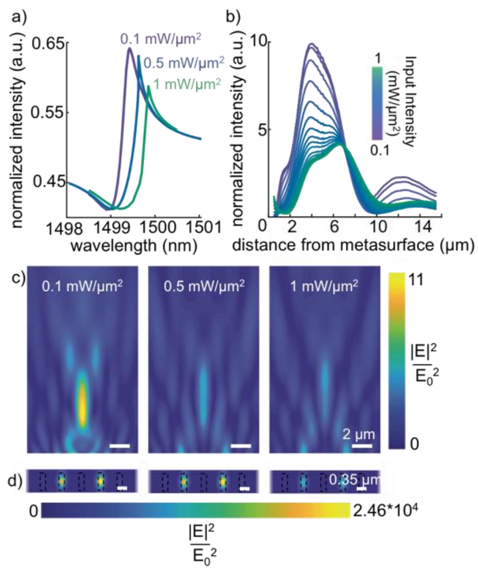

Figure 5: Nonlinear lens response. a) Spectra calculated at the focal spot for input intensities of 0.1 mW/μm^2, 0.5 mW/μm^2, and 1 mW/μm^2, b) focal response in the propagation direction (along the z axis above the high-Q metasurface) for various input intensities, revealing a shift of the focal length with increasing power. All plots are at a wavelength of 1499.4 nm. c) $|E(r)|^2$ field plot for the nonlinear lens with input intensities of 0.1 mW/μm^2, 0.5 mW/μm^2, and 1 mW/μm^2 d) near field profiles within a section of the metasurface for the same powers and wavelengths shown in (c).

As the incident power on the metalens increases, the inherent nonlinear Kerr effect modifies the local permittivity of the silicon according to $\varepsilon(r) = \varepsilon_0(\varepsilon_r + \chi^{(3)}|E(r)|^2)$; here, E(r) is the local electric field strength, $\chi^{(3)}$ is the third-order nonlinear susceptibility (which for silicon is $\approx 2.79 \times 10^{-18} m^2/V^2$), and ε_r and ε_0 are the first-order permittivity of Si and vacuum, respectively. As the intensity increases from 0.1 mW/μm^2 to 1 mW/μm^2, we observe a redshift of the high-Q resonance from 1499.4 nm to 1499.9 nm, as shown in Figure 5a. This shift corresponds to a significant decrease in the far field enhancement of the focal spot at λ=1499.4 nm, as the maximum of the low-power Fano resonance transitions to a minimum at high power. A resulting decrease of over 50% in the normalized focal intensity is observed with increasing input intensity. A spatial change in the focal spot is also observed (Figure 5b). The focal intensity maximum shifts from 3.9 μm for an input intensity of 0.1 mW/μm^2 to 6.55 μm for an input intensity of 1 mW/μm^2. Additionally the overall focal spot position shifts by ~1.2 μm for the place the focal spot begins and ~2.3 μm for the place the focal spot ends, as input intensity increases.

The focusing power of the metalens at 1499.4 nm for low (0.1 mW/μm^2), mid (0.5 mW/μm^2), and high (1 mW/μm^2) input intensities is plotted in Figure 5c. These figures illustrate the power-limiting behavior for the nonlinear lens and the focal length shift. Based on the observed spectral resonance shifts and the onset of an appreciable power-limiting response, we estimate 0.1 mW/μm^2 as the nonlinear threshold, which saturates after approximately 1 mW/μm^2. As with similar high-Q resonant structures, the efficiency of the nonlinear response is increased by at least 2 orders of magnitude, which reduces the necessary input powers to be experimentally reasonable.

Here we discussed a singly resonant system, where only 2 nanobars out of 25 are needed to exhibit a GMR and induce an appreciable high-Q far-field response. As our high-Q scheme is extremely flexible, we can tune the resonant wavelengths and high Q strength of our metasurface by changing either the nanobar or the perturbation geometry. We can further capitalize on this result via frequency-multiplexing, whereby multiple high-Q resonances can be simultaneously achieved by perturbing multiple pairs of nanobars, which was demonstrated in our publication.

In summary, we have developed the first high-Q metasurface lens that leverages its intrinsic nonlinear optical response for power-dependent modulation. Our design combines a diffractive metasurface with a high-Q guided mode resonance to enable efficient nonlinearities. With this metasurface, we show a near-infrared power limiting-like response as well as changes in the focal spot of the lens. The design works at either a single wavelength or at multiple resonant wavelengths spanning the near-infrared. These high-Q metalenses will readily translate to a suite of dynamic imaging platforms, including LIFI, LIDAR, and wavefront sensing.

3. Self-isolated lasing

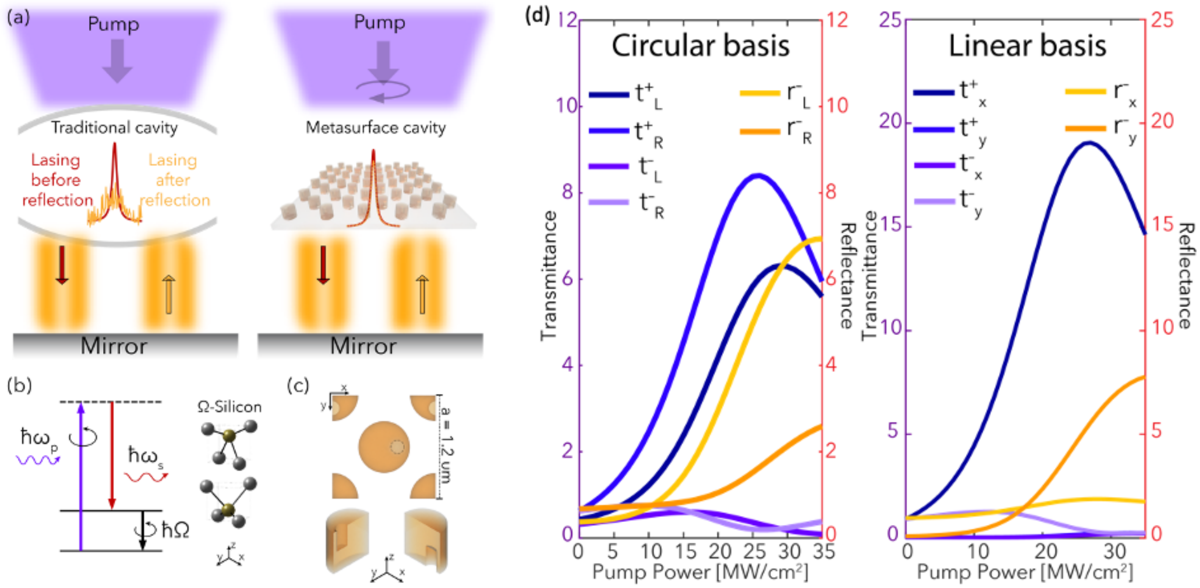

Figure 6: *(a) Schematic of self-isolated metasurface laser. The Raman pump (purple) results in stimulated emission at the Stokes frequency (yellow). Left: In a traditional laser cavity, the original lasing mode (red) is destroyed when reflected light re-enters the cavity(yellow). Right: Due to spin-selective modal restriction of the metasurface cavity, the lasing mode remains undisturbed upon reflection. (b) Energy diagram for Raman decay of a pump photon into a Stokes photon and a phonon, with a schematic of phonon vibration in silicon excited by a circularly-polarized pump. (c) The chiral metasurface, comprised of cylinders in a dimer unit cell arranged in a square lattice with periodicity a = 1.2 µm and antisymmetric notches. (d) Transmittance and reflectance of the signal as a function of the pump power with a left-handed circularly-polarized pump. The signal is polarized in a circularly-polarized basis (left) and linearly-polarized basis (right) and propagates in the -z-direction. The forward direction (+) is defined in the direction of the Raman pump, with transmission (t) and reflection (r) defined accordingly.*

Coherent light sources are foundational to the operation of photonic networks, but their operation requires the use of bulky optical isolators (>1 mm), making small-scale, densely integrated photonic networks infeasible. These isolators prevent light that is reflected along the signal path from re-entering the laser cavity, which would otherwise amplify spurious reflected modes and destroy the light source. A functioning optical isolator must then: i) break reciprocity for a time-reversed pair of modes and ii) restrict all other modes from re-entering the cavity.

We demonstrated a new approach to isolate integrated light sources by tailoring the modal properties of the lasing cavity itself, specifically using a spin-selective chiral metasurface cavity excited with spin-polarized stimulated Raman scattering (Figure 6). Using full-field electromagnetic simulations, we explored a silicon metasurface composed of notched antisymmetric cylinders resonant in the near-infrared. By manipulating the local electromagnetic coupling in a dimer unit cell of notched silicon cylinders, we achieved a chiral optical response with a spin-selective transmittance for left-handed circularly-polarized light >600x greater than the transmittance of right-handed circularly-polarized light. We demonstrated that this high-Q chiral resonance supports Raman lasing, and when the Raman bias is circularly-polarized, the silicon inherits an asymmetric permittivity that mimics the magnetic bias in a Faraday isolator and explicitly breaks reciprocity. Consequently, a signal beam at a frequency Stokes-shifted from the Raman pump is only amplified when the signal obeys photon-phonon spin selection rules imposed by the Raman pump in addition to separate spin selection rules imposed by the symmetry of the chiral metasurface (Figure 6a,b). A signal with a given polarization state transmits with amplification in one direction, but its reflection is suppressed by approximately an order of magnitude in the metasurface cavity, resulting in a self-isolated lasing mode.

A schematic of the metasurface is shown in Figure 6c. The unit cell of the metasurface array is composed of two silicon (n = 3.45) cylinders in a square lattice, each 600 nm tall and 600 nm in diameter with a lattice periodicity of 1.2 µm. Antisymmetric notches 160 nm in diameter bore halfway down the height of the cylinders and are translated in-plane, orthogonally from one another. The geometry is necessarily three-dimensionally chiral, as a planar chiral geometry will maintain a symmetric response in the forward and backward directions and therefore cannot act as a filter for the same handedness of light from both directions. To achieve a three-dimensionally chiral metasurface, we employed a four-step approach to designing the constituent nanoantennas and unit cell: i) spectrally overlapping the electric and magnetic modes; ii) breaking in-plane mirror symmetry to couple the overlapped modes; iii) eliminating rotational symmetry to reorient the direction of the electric mode relative to the magnetic mode; and iv) breaking the remaining in-plane mirror symmetry to remove all symmetry of the unit cell and induce a spin-selective response. To the best of our knowledge, full three-dimensional chirality (i.e. intrinsic asymmetry in which the geometry is non-superimposable on its mirror image), has not been observed in a subwavelength/non-diffracting dielectric metamaterial system.

The metasurface becomes a self-isolated light source when a circularly-polarized pump bias is introduced. In particular, we utilize spin-polarized stimulated Raman scattering (SRS) to explicitly break Lorentz reciprocity. Pumping a Raman-active crystal with sufficiently intense light results in the spontaneous creation of a phonon, which generates a Stokes-shifted spectral sideband. Introducing a second light source at the sideband frequency stimulates this process, resulting in Raman amplification of this second, signal beam. This process defines stimulated Raman scattering and Raman lasing. Considering stimulated Raman scattering in a spin-polarized basis, spin selection rules arise for photon-phonon interactions that dictate when simulated emission occurs. This condition is met in silicon for pump and signal beams of opposite handedness when propagating in the same direction, which we refer to as the forward direction. While a spin-polarized Raman bias is sufficient to achieve nonreciprocal gain for a time-reversed pair of modes, a signal propagating in the backward direction will still experience gain if the signal is not polarized with the appropriate handedness, as is the case upon reflection of the signal. However, in a three-dimensionally chiral metasurface, the modes which correspond to the Raman forbidden polarization are restricted from exciting the cavity.

The resulting isolator-like behavior and nonreciprocal lasing is described in Figure 6d. We fix the pump to be L-CP and observe transmission (t) and reflection (r) of the signal as we vary the pump power. Looking first to the origin where the pump power is completely off, the difference in transmittance between a L-CP and R-CP signal is due strictly to the polarization-selectivity of the chiral metasurface. We also observe a difference in transmittance between a x- and y-polarized signal from the polarization-selectivity of the metasurface. This is not surprising, however, as intrinsic chirality exhibits both circular birefringence and linear birefringence. The signal behavior beyond this point cannot be ascribed to either the polarization-selectivity of the chiral metasurface or to the spin-selection rules alone, but it is rather a convolution of these two effects. For completeness, we plot the lasing action for both a circularly-polarized and linearly-polarized signal, but we refer to the linearly-polarized signal for convenience. We begin to observe amplification of an x-polarized signal in the forward direction (t_x^+) and suppression of its reflection (r_x^+) starting around 2 MW/cm^2. Here, a y-polarized signal in the forward direction is not amplified appreciably (t_y^+), and neither x- nor y-polarized signals are significantly transmitted in the backward direction ($t_{x,y}^-$). Next, we consider reflections of the forward-propagating signals representing mirror reflection of the Raman-amplified lasing mode back into the cavity. The y-polarized signal does not experience gain, and the x-polarized signal experiences roughly an order of magnitude less gain than its forward-propagating transmitted counterpart at a pump power of 16 MW/cm^2. Accordingly, our three-dimensional chiral metasurface is capable of self-isolated lasing.

In summary, we developed a submicron lasing cavity with a nonzero chirality parameter and asymmetric permittivity that, together, impose isolation on the lasing mode emitted from that cavity. Here, optical isolation is not considered as an additional photonic component but as a feature built natively into the light source itself. Importantly, we break Lorentz reciprocity with a spin-polarized Raman bias that avoids dynamic reciprocity, which has no lower size limit and can be applied to a wide array of dielectric materials. We also develop a general methodology for designing intrinsic chirality in a subwavelength dielectric platform, which opens access to chiral near-field interactions that cannot be achieved in planar chiral systems. Beyond subwavelength nonreciprocal and multifunctional integrated light sources, our three-dimensional chiral metasurface could also enable advances in topological photonics and nanophotonic sensing platforms.

Awards, 2018-2019

- D. Barton –Intelligence Community Postdoctoral Fellowship
- D. Barton – MRS Graduate Student Award
- J. Dixon – Kodak Fellowship
- J. Dionne – Alan T. Waterman Award
- J. Dionne – NIH New Innovator Award
- E. Klopfer – NSF Fellowship
- Sahil Dagli - NSF Fellowship and NDSEG Fellowship

Publications, 2018-present

- M. Lawrence*, D. Barton*, J. Dixon, et al, J. Dionne. "High-quality factor phase gradient metasurfaces," *Nature Nanotechnology* (2020)
- Elissa Klopfer*****, Mark Lawrence, David R. Barton III, Jefferson Dixon and Jennifer A. Dionne*****, Dynamic Focusing with High-Quality-Factor Metalenses, *Nano Letters* 20, 5127 (2020)
- M. Lawrence and J. Dionne, "Nanoscale nonreciprocity via photon-spin-polarized stimulated Raman scattering," *Nature Comm.* 10, 3297 (2019)
- M. Solomon, J. Hu, M. Lawrence, A. Garcia-Etxarri, and J. Dionne, "Enantiospecific Optical Enhancement of Chiral Sensing and Separation with Dielectric Metasurfaces", *ACS Photonics* 6, 43 (2019)
- Jack Hu, Mark Lawrence, and Jennifer A. Dionne, "High Quality Factor Dielectric Metasurfaces for Ultraviolet Circular Dichroism Spectroscopy," *ACS Photonics* 7 (2020)
- J. Dixon, M. Lawrence, D. Barton, and J. Dionne, "Self-isolated Raman lasing with a chiral dielectric metasurface," *PRL,* in revisions (2020
- E. Klopfer, M. Lawrence, D. Barton, J. Dixon, S. Dagli, and J. Dionne. "Nonlinear modulation of high-Q metalenses," in preparation (2020)

Summary of Results, All Years (2014-2019):

25 Publications and over 100 Invited Presentations from 2014-present:

- Publications include two in Nature Nanotechnology, two in Nature Materials, and four in Nature Communications
- Presentations include a Plenary Lecture at the International Microscopy Congress, five Gordon conference presentations, and a TED-X talk

3 Industry collaborations and 3 International collaborations emerging from PECASE funding:

- Northrop Grumman, Seagate, Intel
- Albert Polman (FOM-AMOLF); Javier Aizpurua (DIPC); N. Zheludev (NTU, Singapore)

17 Major Awards:

- J. Dionne: Waterman Award, Moore Inventor Fellow, MRS Young Investigator, Adolf Lomb Medal, Nano Letters Young Investigator, Sloan Fellowship, Dreyfus-Teacher Scholar Award

- Student Awards: MRS Graduate Student Award (Hadiseh Alaeian, David Barton); SPIE Outstanding student award finalist (David Barton); Chevron fellow (David Barton); Work Featured in ITRS Roadmap (Brian Baum); Huggins award for best Materials Science Ph.D. (Tarun Narayan); Kodak Fellowship (Jefferson Dixon); NSF Fellowship (Elissa Klopfer and Sahil Dagli); NDSEG Fellowship (Sahil Dagli)

3 Centers based on PECASE research:

- Catalyst for Collaborative Solutions (J. Dionne, PI): a 6-PI Center on Bacterial Detection spanning Stanford's Schools of Engineering, Medicine, Business, and the VA-Palo Alto
- DOE-EFRC (J. Dionne, PI): a 12-PI Center on Photonics at Thermodynamic Limits spanning Stanford, Berkeley, Caltech, UIUC, and Harvard
- Stanford Photonics Research Center (J. Dionne, faculty co-Director): a multi-PI Center linking Stanford faculty to companies including Corning, Seagate, Hamamatsu, Pfizer, and Google

Key Accomplishments, 2014-2019

Design of nanoscale optical diodes: We have designed nanoscale metasurfaces that enable non-reciprocal free space filtering and wave-front shaping. By patterning ultrathin (<100nm thick) Si films with subtle notches, resonant modes emerge with very high quality factors, amplifying the local electric field strength and thus reducing the threshold for nonlinear phenomena, such as Si's nonlinear Kerr effect. We have shown that asymmetries in the notch pattern can suppress the strong field amplification from one side, leading to a directionally dependent redshift of the modes and, ultimately, nonreciprocal transmission. Diode action, i.e. zero transmission from one side and high transmission from the other, can be achieved for reasonable input powers of ~10 kW/cm^2, over an optical path length of just 100nm. We have also shown that this concept can be extended to the diffractive regime to achieve nonreciprocal anomalous refraction. (M. Lawrence, D. Barton, J. Dionne, Nano Letters 2018)

Design of nanoscale optical isolators: We have shown how stimulated Raman Scattering can enable nanoscale optical isolation by using spin selective photon-phonon interactions. In particular, we show how Raman amplification with circularly polarized light is, rather than simply asymmetric, forbidden for one incident direction - a consequence of an angular momentum conserving spin selection rule. Then, exploiting the local nature of chiral SRS, we design nanoscale antennas which both dramatically enhance and maintain the circulation of near-infrared chiral light, culminating in nanoscale Raman-based isolation. We benchmark this process with two deeply subwavelength structures: nonreciprocal Si metasurfaces and diamond-loaded plasmonic nanoantennas. Importantly, no special symmetries are required of the mediating crystal since a spinning photon can be imprinted on almost any Raman active phonon; consequently, a host of traditional and emerging materials are available for constructing photon-spin-polarized SRS-based nonreciprocal devices. (M. Lawrence and J. Dionne, Nat. Comm. 2019 and J. Dixon, M. Lawrence, D. Barton, and J. Dionne, PRL, in revisions, 2020)

The first high-quality factor phase gradient metasurfaces: We have experimentally demonstrated the highest quality factor ever observed in a phase gradient metasurface. As the dimensions of dielectric cavities are reduced to subwavelength scales, their resonant modes begin to scatter light into many spatial channels. Such enhanced scattering is a powerful tool for light manipulation, but also leads to high radiative loss rates and commensurately low *Q*-factors, generally of order ten. We proposed and experimentally demonstrated a strategy for the generation of high *Q*-factor resonances in subwavelength-thick phase gradient metasurfaces. By including subtle structural perturbations in individual metasurface elements, resonances are created that weakly couple free-space light into otherwise bound and spatially localized modes. Our metasurface can achieve *Q*-factors >2,500 while beam steering light to particular directions. High-*Q* beam splitters are also demonstrated. With high-*Q* metasurfaces, the optical transfer function, near-field intensity and resonant line shape can all be rationally designed, providing a foundation for efficient, free-space-reconfigurable and nonlinear nanophotonics. (M. Lawrence, D. Barton, J. Dionne, et al, Nat. Nanotechnology 2020)

Design of PT-symmetric plasmonic apertures for polarization rotation: Control of the polarization state of light is essential for many technologies, but is often limited by weak light-matter interactions that necessitate long device path lengths or significantly reduce the signal intensity. We designed a nanoscale plasmonic aperture capable of modifying the polarization state of far-field transmitted light without loss in the probe signal. The aperture is a coaxial resonator consisting of a dielectric ring embedded within a metallic film; parity-time (PT) -symmetric inclusions of loss and gain within the dielectric ring enable polarization control. Since the coaxial aperture enables near-thresholdless PT-symmetry breaking, polarization control is achieved with realistic levels of loss and gain. Exploiting this sensitivity, we show that the aperture can function as a tunable waveplate, with the transmitted ellipticity of circularly polarized incident light changing continuously with the dissipation coefficient from $\pi/2$ to 0 (i.e., linear polarization). Rotation of linearly polarized light with unity efficiency is also possible, with a continuously tunable degree of rotation. This compact, low-threshold, and reconfigurable polarizer may enable next-generation, high-efficiency displays, routers, modulators, and metasurfaces. (B. Baum, M. Lawrence, D. Barton, H. Alaeian, and J. Dionne, PRB 98, 2018)

*Design of broadband non-Hermitian metamaterials:*We theoretically demonstrated non-Hermitian metamaterial exhibiting broadband and wide-angle nonreciprocity. The metamaterial consists of planar metal-dielectric layers with a parity-time (PT) symmetric distribution of loss and gain. With increasing loss and gain, the band structure and band gap are strongly modified; further, the PT potential leads to distinct internal field distributions when illuminated from different sides. Including nonlinearities arising from natural loss and gain saturation leads to nonreciprocal transmission in the visible over a 50-nm wavelength and $\pm 60\circ$ angular range. (D. Barton, M. Lawrence and J. Dionne, PRB 97, 2018)

Enantioselective optical trapping: As an example of non-Hermitian plasmonic metamaterials, we have designed nanoscale coaxial resonators that enable enantioselective optical trapping. While reciprocal, these structures enable asymmetry in the optical forces they generate. In particular, our coaxial plasmonic tweezers can selectively trap nano-specimens based on their chirality. By devising a new technique, termed chiral-optical force microscopy (COFM), we visualized such enantioselective forces in three-dimensions with pico-Newton sensitivity and 2 nm spatial resolution. This platform provides an all-optical routes to trapping and sorting racemic mixtures of molecules for high-sensitivity molecular sensing, and pharmaceutical and agrochemical chemical purification. (Y. Zhao, J. Dionne, et al., Nature Nanotechnology, 2017)